Acta Pharmaceutica Sinica B 2019;9(5):1050−1060

Chinese Pharmaceutical Association
Institute of Materia Medica, Chinese Academy of Medical Sciences

Acta Pharmaceutica Sinica B

www.elsevier.com/locate/apsb
www.sciencedirect.com

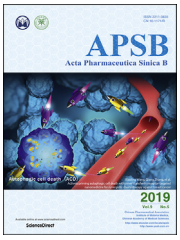

ORIGINAL ARTICLE

Injectable peptide hydrogel as intraperitoneal triptolide depot for the treatment of orthotopic hepatocellular carcinoma

Xiyue Zhao[a,b,†], Xiaoyu Liu[b,†], Pengcheng Zhang[b,c,e,*], Yiran Liu[b,f], Wei Ran[b,e], Ying Cai[b,e], Junyang Wang[b,g], Yihui Zhai[b,e], Guanru Wang[b], Yaping Ding[a], Yaping Li[b,d,e,*]

[a]*Department of Chemistry, Shanghai University, Shanghai 200444, China*
[b]*State Key Laboratory of Drug Research & Center of Pharmaceutics, Shanghai Institute of Materia Medica, Chinese Academy of Sciences, Shanghai 201203, China*
[c]*Yantai Key Laboratory of Nanomedicine & Advanced Preparations, Yantai Institute of Materia Medica, Yantai 264000, China*
[d]*School of Pharmacy, Yantai University, Yantai 264005, China*
[e]*University of Chinese Academy of Sciences, Beijing 100049, China*
[f]*Nano Science and Technology Institute, University of Science and Technology of China, Suzhou 215123, China*
[g]*Jilin University, Changchun 130012, China*

Received 17 April 2019; received in revised form 10 May 2019; accepted 20 May 2019

KEY WORDS

Abstract Chemotherapy is among the limited choices approved for the treatment of hepatocellular carcinoma (HCC) at intermediate and advanced stages. Preferential and prolonged drug exposure in diseased

Abbreviations: Akt, protein kinase B; ANOVA, analysis of variance; AST, aspartate transaminase; ATL, alanine transaminase; AUC_{0-13}, areas under the curve; AURKA, aurora A kinase; Bel-7402/Luc, luciferase transfected human HCC cell line Bel-7402; BUN, blood urea nitrogen; CAS, Chinese Academy of Sciences; CD, circular dichroism; CKS2, cyclin kinase subunit-2; CRE, creatinine; C_{16}-N, C_{16}-GNNQQNYKD-OH; C_{16}-N/DiI, DiI-labeled C_{16}-N; C_{16}-N/DiR, DiR-labeled C_{16}-N hydrogel; C_{16}-N/T, triptolide-loaded peptide amphiphile-based hydrogel; DL, drug loading; D-Luciferin, (*S*)-4,5-dihydro-2-(6-hydroxy-2-benzothiazolyl)-4-thiazolecarboxylic acid potassium; DSPE-PEG, 1,2-distearoyl-*sn*-glycero-3-phosphoethanolamine-*N*-[amino (polyethylene glycol)-2000]; DSPE-PEG/DiI, DiI-labeled DSPE-PEG; DSPE-PEG/DiR, DiR-labeled DSPE-PEG micelle; DSPE-PEG/T, drug-loaded DSPE-PEG micelles; EE, encapsulation efficiency; FBS, fetal bovine serum; FI, fluorescence intensity; FI range, fluorescence intensity range; GEMOX, gemcitabine and oxaliplatin; H&E, hematoxylin and eosin; HFIP, 1,1,1,3,3,3-hexafluoro-2-propanol; HPLC, high-performance liquid chromatography; LC−MS, liquid chromatography−mass spectrometry; OB glue, EPIGLUs; RFI, relative fluorescence intensity; TACE, transarterial chemoembolization; TEM, transmission electron microscopy; TIR, tumor inhibition rate; T_{max}, time to reach highest fluorescence intensity.

*Corresponding authors. Tel./fax: +86 21 20231979.
E-mail addresses: pzhang@simm.ac.cn (Pengcheng Zhang), ypli@simm.ac.cn (Yaping Li).

†These authors made equal contributions to this work.

Peer review under responsibility of Institute of Materia Medica,Chinese Academy of Medical Sciences and Chinese Pharmaceutical Association.

https://doi.org/10.1016/j.apsb.2019.06.001

Self-assembly;
Hydrogel;
Peptide amphiphile;
Triptolide;
Hepatocellular carcinoma

sites is required to maximize the therapeutic index of the drug. Here, we report an injectable supramolecular peptide hydrogel as an intraperitoneal depot for localized and sustained release of triptolide for the treatment of orthotopic HCC. We chose peptide amphiphile C_{16}-GNNQQNYKD-OH-based nanofibers as gelators and carriers for triptolide. Sustained triptolide release from the hydrogel was achieved over 14 days *in vitro*, with higher accumulation in and cytotoxicity against human HCC Bel-7402 in comparison with L-02 fetal hepatocytes. After intraperitoneal injection, the hydrogel showed prolonged retention over 13 days and preferential accumulation in the liver, realizing HCC growth inhibition by 99.7 ± 0.1% and animal median survival extension from 19 to 43 days, without causing noticeable pathological changes in the major organs. These results demonstrate that injectable peptide hydrogel can be a potential carrier for localized chemotherapy of HCC.

1. Introduction

Liver cancer is the second leading cause of cancer-related death worldwide, resulting in more than 810,000 deaths in 2015, and the mortality was continuously growing in the past 25 years[1]. Hepatocellular carcinoma (HCC) accounts for about 70%−90% of all primary liver cancer[2]. HCC of early stage is eligible for curative therapies such as resection, transplantation and local ablation, with median survival time over 60 months[3]. Unfortunately, most HCC patients have already developed local (intermediate stage) or portal vein (advanced stage) invasion at their first time of diagnosis, with 5-year survival rates of only 11% and 3%, respectively[4]. Transarterial chemoembolization (TACE) using drug-eluting beads is now a standard treatment for intermediate stage HCC patients, and profoundly increases 5-year survival rate to 22.5%[5]. While significantly alleviates the systemic side effects of chemotherapy, TACE requires imaging-guided surgery performed by an experienced doctor, and the subsequent blood vessel blockage hampers potential combination therapy with substantial damages to local liver tissues[5]. For patients with advanced HCC, sorafenib and pembrolizumab are two available treatments in the clinic. Sorafenib prolonged the median time to radiologic progression to 5.5 months from 2.8 months of non-treated patients, with no complete and 2% partial response recorded[6], while patients receiving pembrolizumab showed 1% complete and 16% partial responses[7]. Systemic chemotherapy with gemcitabine and oxaliplatin (GEMOX) has also been evaluated in the clinic on advanced HCC patients with a response rate of 22%, and tumor shrinkage was observed in some of the patient[8]. However, more than 50% of the patients did not respond to the treatments, and these systemically administrated drugs all elicited grade 3 or 4 toxicity in ~10%−44% patients due to off-target drug exposure[6−8]. In addition to these drugs that are either approved or in clinical trials, other compounds are also under intensive investigation at the preclinical stage. For instance, triptolide is a potent anti-tumor agent which kills cancer cells through heat shock gene (*e.g.*, heat shock protein 70) expression inhibition, protein kinase B (Akt)/mammalian target of Rapamycin/p70S6K pathway inactivation, or cyclin kinase subunit-2 (CKS2) and aurora A kinase (AURKA) down-regulation[9−11]. Triptolide was found to be more potent than doxorubicin and sorafenib against a panel of HCC cells *in vitro*, but it only stabilized the disease *in vivo*, probably due to limited drug exposure and severe systemic toxicity[11]. Therefore, new drug delivery systems that can realize prolonged and preferential drug accumulation in HCC tumor are still of urgent need.

Nanomedicine can significantly modify the pharmacokinetics of encapsulated drugs[12,13], and it has been found that majority of intravenously injected nanoparticles accumulated in the liver. However, detailed investigations showed that these particles are mainly captured by Kupffer cells, B cells and endothelial cells[14]. An extensive screen is necessary to identify ligands that could direct cargos specifically to HCC cells rather than hepatic cell and immune cells *in vitro*[15,16], and a stimuli-responsive drug release in the HCC was also found to be essential[17−19]. However, the efficiency of these nanomedicines may be compromised by the formation of protein corona *in vivo*[20]. Therefore, it is still challenging to maintain a steady and optimized drug exposure in the liver. Intraperitoneal chemotherapy is an alternative strategy to treat cancers that are confined to the peritoneal cavity[21]. Intraperitoneal chemotherapy may be also advantageous in treating portal-vein-perfused micrometastatic cancer in the liver which was characteristic for intermediate and advanced HCC[21,22]. To prolong drug retention in the peritoneal cavity, the use of drug-loaded nanoparticles was explored[23]. Intraperitoneal injection of bioadhesive nanoparticles has been further explored by Zhao et al.,[24] in the aim of slowing nanoparticle clearance through lymphatic draining and realizing *in situ* release of encapsulated drug for localized therapy[25,26]. Nevertheless, readily drug release from nanoparticles is routinely observed because of their high specific surface area, resulting in faster clearance of the drugs prior to their nanocarriers.

Hydrogel is able to retard drug release by physically limiting material exchange between immobilized content with outside environment[27]. For instance, tunable drug release from liposomes has been achieved by varying the extent of crosslinking of the hydrogel[28], and prolonged drug exposure (14 days) in peritoneal cavity was observed when the hybrid system was used[29]. In comparison with cross-linked polymeric hydrogels, supramolecular polymeric hydrogels composed of peptide derivatives receive increasing interest, because of their shear-thinning property and biocompatibility[30−33]. More importantly, the capability of these

supramolecular peptide hydrogels in controlling drug release is not compromised[33–35]. These hydrogels could be successfully prepared with peptides of different molecular weights ranging from >100 kDa elastin-like peptides[36] and block-polypeptides[37] to small dipeptide[38] and tripeptide[39]. Peptides of different secondary structures including coiled coil[40,41], hairpin[33,42], and β-sheet[43,44], are all able to form hydrogels. Regardless of their difference in composition and secondary structure, most of these peptide hydrogelators self-assembled into one-dimensional fibrils, which further entangled with each other through salt bridge, hydrogen bond, and electrostatic attraction to form three-dimensional networks and therefore hydrogels[40,45–47]. Additional functional groups such as targeting ligands[48], enzyme-responsive groups[49–51], drugs[52,53], fatty acids[54,55], DNA[56], chelator[57], fluorophores[58] can be integrated into peptide gelators without disturbing their capability in hydrogel formation. These peptide-based hydrogels have found broad biomedical applications in areas, such as tissue engineering[59], drug delivery[60] and imaging[58,61].

In our previous study, an injectable peptide amphiphile-based hydrogel, namely C_{16}-GNNQQNYKD-OH (C_{16}-N), has been identified, and the losartan-loaded hydrogel showed sustained drug release after intratumoral injection with potent activity in cancer-associated fibroblast inhibition[54]. Given its biocompatibility and sustained drug release in the site of injection, herein, an injectable and triptolide-loaded peptide amphiphile-based hydrogel (C_{16}-N/T) is prepared through co-assembly strategy (Fig. 1A). The influence of triptolide encapsulation on the physicochemical properties of the hydrogel was determined, and sustained drug release from the hydrogel was monitored *in vitro* and *in vivo*. The anti-tumor activity and toxicity were also evaluated on HCC cells and normal hepatic cells *in vitro*, and on orthotopic mice model *in vivo*. C_{16}-N/T significantly retarded the growth of the tumor and prolonged the survival of mice (Fig. 1B). Our findings highlight the importance of spatiotemporal control of drug exposure in maximizing efficacy and minimizing side effects, and indicate that supramolecular peptide hydrogel could be a feasible drug delivery system for drugs against HCC.

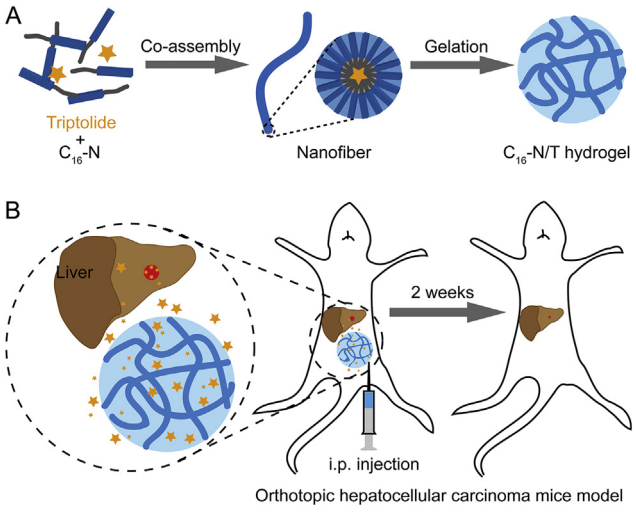

Figure 1 Schematic illustration of the preparation and mechanism of action of C_{16}-N/T. (A) C_{16}-N/T was prepared by a co-assembly strategy. (B) After intraperitoneal injection, sustained triptolide release and accumulation in the liver could be achieved, which led to growth inhibition of othortopic hepatocellular carcinoma tumor (HCC).

2. Materials and methods

2.1. Materials and animals

Fmoc-Asp(O*t*Bu)-Wang resin and Fmoc-protected amino acids were all obtained from GL Biochem (Shanghai, China). Other reagents used in solid-phase peptide synthesis such as *N*,*N*-diisopropylethylamine, *O*-benzotriazole-*N*,*N*,*N*,*N*-tetramethyluronium trifluoroacetic acid, hexafluorophosphate, 1,1,1,3,3,3-hexafluoro-2-propanol (HFIP) and triisopropylsilane were purchased from J&K (Shanghai, China). Triptolide (>98%) was purchased from Desite Biotechnology Co., Ltd. (Chengdu, China). 1,2-Distearoyl-*sn*-glycero-3-phosphoethanolamine-*N*-[amino (polyethylene glycol)-2000] (DSPE-PEG) was acquired from A.V.T (Shanghai) Pharmaceutical Co., Ltd. Alexa Fluor® 594-conjugate AffiniPure Donkey Anti-Rabbit lgG was purchased from Jackson ImmunoResearch Inc. (West Grove, USA). F4/80 (D4C8V) XP® Rabbit mAb was bought from Cell Signaling Technology Inc. (Boston, USA). DiR and DiI dyes were obtained from Meilun Biotech (Dalian, China). EPIGLUs (OB glue) were obtained from MEYER-HAAKE Gmbh (Germany). (*S*)-4,5-Dihydro-2-(6-hydroxy-2-benzothiazolyl)-4-thiazolecarboxylic acid potassium (D-Luciferin) was bought from Yeasen (Shanghai, China). Unless noted otherwise, all other reagents were obtained from Sinopharm Chemical Reagent Co., Ltd. (Shanghai, China).

Luciferase transfected HCC cell line Bel-7402/Luc and human fetal hepatocyte cell line L-02 were provided by Shanghai Cell Resource Center of Shanghai Institute for Biological Sciences, Chinese Academy of Sciences (CAS, China). Both cell lines were cultured with RPMI 1640 Medium (Invitrogen, Carlsbad, USA) supplemented with 10% fetal bovine serum (FBS, Invitrogen, Carlsbad, USA) and 1% Penicillin–Streptomycin solution (Meilun Biotech, Dalian, China). Cells were kept in a humidified incubator containing 5% CO_2 at 37 °C.

Female Balb/c nude mice (18−20 g) were purchased from Shanghai Experimental Animal Center (Shanghai, China). All animal experiments were approved by the Institutional Animal Care and Use Committee of the Shanghai Institute of Materia Medica, Chinese Academy of Sciences (China).

2.2. Peptide synthesis

Peptide amphiphile C_{16}-N was synthesized and purified according to our reported procedures[54]. Mass spectrometry and analytical high-performance liquid chromatography (HPLC) were used to confirm the molecule mass and purity of the obtained material, respectively.

2.3. Triptolide encapsulation

A co-assembly method was used to encapsulate triptolide into the hydrogel. Briefly, C_{16}-N (5 mmol/L) was mixed with triptolide in HFIP at different molar ratios (2:1, 5:1, 10:1, 25:1, and 50:1, C_{16}-N-to-triptolide). HFIP was then removed under vacuum, and the remaining was rehydrated with deionized water (~1 mmol/L in peptide amphiphile, pH 7.4) under sonication. The solutions

were allowed to age overnight before centrifugation (12,000×*g*, 5 min, 4 °C), and the supernatants were transferred into pre-weighted vials for lyophilization. The amounts of encapsulated triptolide in the reconstituted lyophilisates were determined by HPLC (Waters, Milford, USA) equipped with an XBridge™ BEH130 C18 column (5 μm, 150 mm × 4.6 mm), which was eluted by a mixture of water and acetonitrile (flow rate: 1 mL/min; acetonitrile gradient: from 10% to 90% over a period of 17 min; wavelength: 220 nm). The drug loading (DL) and encapsulation efficiency (EE) was calculated with Eq. (1) and Eq. (2):

$$\mathrm{DL}\,(\%) = \frac{W_{\text{recovered drug}}}{W_{\text{recovered lyophilisate}}} \times 100 \quad (1)$$

$$\mathrm{EE}\,(\%) = \frac{W_{\text{recovered drug}}}{W_{\text{added drug}}} \times 100 \quad (2)$$

2.4. Transmission electron microscopy (TEM)

C_{16}-N or C_{16}-N/T hydrogel (C_{16}-N: 10 mmol/L) was instantly diluted to 500 μmol/L before sample preparation. Seven microliters of C_{16}-N or C_{16}-N/T solution (500 μmol/L in water) was deposited onto a carbon-film-coated copper grid. Excess solution was removed using filter paper to form a thin layer, and the sample was negatively stained using uranyl acetate (2% *w/v*). After being air dried at room temperature for 3 h, the samples were imaged on an FEI Tecnai 12 TWIN electron microscope (120 kV) accompanied with an SIS Megaview III wide-angle CCD camera.

2.5. Circular dichroism (CD)

To understand whether the secondary structure of C_{16}-N was affected by drug encapsulation, CD spectra (190−400 nm) of C_{16}-N/T (500 μmol/L in water, 50:1 C_{16}-N-to-triptolide), C_{16}-N (500 μmol/L in water) and free triptolide (10 μmol/L in methanol) were recorded on a JASCO J-810 spectropolarimeter (Japan), using water or methanol as references, respectively. The corrected signal was then converted from ellipticity (mdeg) to mean molar ellipticity (deg·cm^2/dmol).

2.6. Hydrogel formation

Hydrogel was prepared by mixing 9 parts of C_{16}-N or C_{16}-N/T (>10 mmol/L in peptide amphiphile in water, pH 7.4) with one part of 10 × PBS through vortex. The hydrogel formation and shear-thinning property of the mixture were determined using inverted-vial test. The effects of salt, drug encapsulation and shear force on the viscosity of the hydrogels were investigated with Anton Paar MCR 101 rheometer (Anton PaarTrading Co., Ltd., Shanghai, China) equipped with a stainless-steel parallel plate measuring system (50-mm plate diameter).

2.7. Drug release

Release profiles of triptolide from C_{16}-N/T hydrogel and drug-loaded DSPE-PEG micelles (DSPE-PEG/T) were determined using a transwell-based protocol, as we reported previously.[54] C_{16}-N/T (50:1 or 25:1 C_{16}-N-to-triptolide, pH 7.4, 2.5% *w/v* in PBS) was prepared as described above, and DSPE-PEG micelles with the same drug loading were prepared and used as control. Then, 500 μL of each sample was loaded into the donor inserted cells (n = 3 for each group), and allowed to release the encapsulated drug into 1 mL incomplete 1640 medium in the receptor cells (37 °C). The medium in the receptor cells was refreshed at 1, 2, 4, 8, 12 and 24 h in the first day, and the refreshed every day until day 14. The amount of released triptolide in the medium was monitored using HPLC, and the molecular weight of the released triptolide was confirmed with liquid chromatography−mass spectrometry (LC−MS, 6545 Q-TOF, Agilent, Santa Clara, USA). The cumulative triptolide release was plotted against the release time.

To test whether the hydrogel could also control the release of macrobiomolecules, 25 ng Alexa Fluor® 594-labeled IgG was mixed with 50 mg C_{16}-N to form antibody-loaded hydrogel (pH 7.4, 2.5% *w/v* in PBS containing 0.025% sodium azide, *w/v*). The transwell-based protocol described above was used, and 12.5 ng/mL antibody solution was used as a control. Half milliliter of each sample was placed into FBS pre-soaked donor inserted cells (n = 3), and the released antibody was collected in receptor cell containing 1 mL 1640 medium (1% FBS, *v/v*). The release medium was refreshed at 1, 2, 4, 8 and 24 h on the first day, and every two days after that until day 14. The amount of antibody was determined *via* a multimode plate reader (Enspire PerkinElmer, Fremont, USA). The cumulative antibody release was plotted against time of release.

2.8. In vitro cytotoxicity and uptake

We first investigated the cytotoxicity of free triptolide on Bel-7402/Luc and L-02 cells, respectively. Briefly, Bel-7402/Luc or L-02 cells were seed at 6 × 10^3 cells/well in 96-well plates for 24 h, respectively. Cells were then incubated with fresh medium containing various concentrations of triptolide (0.0001, 0.001, 0.01, 0.02, 0.1, 0.2, 1 and 2 μmol/L) for 72 h. The cytotoxicity of the drug was determined using an MTT-based method, according to the manufacturer's protocol.

To test the efficacy of triptolide released from either C_{16}-N/T or DSPE-PEG/T, Bel-7402/Luc or L-02 cells were incubated with diluted (2000 ×) release medium collected at 2 h, day 1, 3 and 11 during release experiment. Dilution was conducted because more drugs were used in the release study than in efficacy study, in order to be quantified using HPLC. The cytotoxicity of triptolide was determined using an MTT-based method 72 h after incubation.

To explore the cellular uptake of the released drug by Bel-7402/Luc or L-02 cells, DiI-labeled C_{16}-N hydrogel and DSPE-PEG micelles were prepared, and an *in vitro* release experiment was conducted under similar conditions as described above. Samples collected at 2 h, day 1, 3 and 11 were incubated 12 h with either Bel-7402/Luc or L-02 cells that had been seeded at 1.5 × 10^5/well in 12-well plates 24 h before the experiment. Intracellular accumulation of DiI was qualitatively observed with an inverted fluorescence microscope attached to a monochromatic CCD camera (Olympus, Tokyo, Japan), and quantitatively determined using Flow cytometry (Calibur, BD Biosciences, Franklin lake, USA).

2.9. Abdominal retention and biodistribution of the hydrogel

Nude mice were assigned into two groups (n = 3), receiving either DiR-labeled C_{16}-N hydrogel (C_{16}-N/DiR, 19 mmol/L) or DSPE-PEG micelle of similar concentration (DSPE-PEG/DiR, 2 mg/kg DiR) through intraperitoneal injection (i.p.). The abdominal retention of either hydrogel or micelle was monitored and analyzed using an IVIS Spectrum imaging system

(PerkinElmer, Fremont, USA) at day 0, 1, 3, 5, 11, and 13 after injection. The total fluorescence intensity was normalized to the highest fluorescence intensity of each group while plotted against time. The two samples were also injected into wells filled with PBS and then imaged with IVIS Spectrum imaging system.

To understand the biodistribution of the injected formulations, nude mice were assigned into one of the three groups ($n = 18$), receiving 100 μL DiR-labeled C_{16}-N (i.p.), DSPE-PEG (i.v.), or DSPE-PEG (i.p.). At 5 min, 1 h, 24 h, 3 days, 6 days, and 13 days after the injection, 3 mice of each group were killed to harvest the major organs and blood, which were be further imaged and analyzed using an IVIS Spectrum imaging system. Organs collected from mice receiving different amount of DiR (in DSPE-PEG/DiR, i.v.) were used as standards, and the fluorescence intensity of the organs were determined using IVIS Spectrum imaging system. The DiR in these organs was then extracted using methanol and determined with a fluorospectrometer (PerkinElmer, Fremont, USA). The fluorescence intensity was then plotted against the concentration of DiR in the tissues.

2.10. Orthotopic HCC mice model

Bel-7402/Luc cells (10^7 cells in 100 μL) were injected subcutaneously into nude mice, and the tumors were harvested when the diameters reached 0.5 cm. The tumors were cut into small blocks (1 mm × 1 mm × 1 mm) in sterilized PBS containing 1% penicillin–streptomycin. The tumor blocks were kept on the ice and used within 1 h. Healthy nude mice were anesthetized with sodium pentobarbital sulfate (i.p., 50 mg/kg), and then fixed on a sterile table with surgical film in supine position. The skin of the abdomen was disinfected with 75% ethanol, and a cut of 1 cm in length was made on the abdominal wall of the mice to expose the left lobe of the liver. The liver was rubbed softly with a cotton swab, and then one tumor block was glued onto the rubbed surface with medical OB glue. After 1 min, the cut was closed with 5-0 suture line and disinfected with iodophor with an additional penicillin injection (i.m.). The mice were kept warm and monitored closely until conscious. Routine sterile feeding was taken post-operation.

To monitor the growth of tumors, D-Luciferin was injected through tail vein (15 mg/mL, 200 μL, i.v.), and the bioluminescence from the tumor was monitored with IVIS Spectrum imaging system at day 13 and day 45 after implantation. The livers were then dissected for further imaging and histological examination.

2.11. Anti-tumor efficacy

To determine the growth profiles of orthotopic HCC after different treatments, animals developed orthotopic HCC (confirmed with IVIS Spectrum imaging system 10 days after implantation) were divided into 5 groups ($n = 3$): C_{16}-N/T (i.p.), DSPE-PEG/T (i.v.), DSPE-PEG/T (i.p.), C_{16}-N (i.p., 180 mg/kg), and PBS (i.v.), and dosed at 1 mg/kg triptolide. The growth of the tumors was monitored and semi-quantified using IVIS Spectrum imaging system before or 1 and 2 weeks after the treatment, and the mice were killed for further liver imaging and histological analysis. The tumor inhibition rate (TIR) of treatment at the end of the experiment was calculated based on the following Eq. (3):

$$\mathrm{TIR}\,(\%) = \left(1 - \frac{\mathrm{RFI}_{\mathrm{treatment}}}{\mathrm{RFI}_{\mathrm{PBS}}}\right) \times 100 \quad (3)$$

In a separate experiment, the survivals of mice bearing orthotopic HCC were also monitored after a single injection with C_{16}-N/T (i.p.), DSPE-PEG/T (i.v.), DSPE-PEG/T (i.p.), C_{16}-N (i.p., 180 mg/kg), or PBS (i.v.) at 1 mg/kg triptolide ($n = 8$ for each group). The body weights of the mice were monitored for 70 days.

2.12. Serum biochemical parameters and histological study

To evaluate the safety of C_{16}-N/T and other formulations, healthy nude mice receiving C_{16}-N/T (i.p.), DSPE-PEG/T (i.v.), DSPE-PEG/T (i.p.), C_{16}-N (i.p.), or PBS (i.v.) were killed to harvest serum and major organs 4 days after the treatment ($n = 3$ for each group). The activities of alanine transaminase (ATL) and aspartate transaminase (AST) and the concentration of blood urea nitrogen (BUN) and creatinine (CRE) in the serum were determined and compared. The major organs were fixed, dehydrated, embedded in paraffin blocks, sectioned, and stained with hematoxylin and eosin (H&E) for histological analysis. Images were captured using an inverted fluorescence microscope attached to a monochromatic CCD camera (IX83, Olympus, Japan).

2.13. Statistical analysis

Each experiment was conducted at least in triplicate, and the data were given as mean ± SD. Data were analyzed using either two-tailed student' *t*-test or one-way analysis of variance (ANOVA) using GraphPad Prism 6.0 software to assess the significance of the difference. Statistical differences were defined as significant when $P < 0.05$.

3. Results and discussion

3.1. Co-assembly and characterization of C_{16}-N/T

C_{16}-N was synthesized, purified and characterized according to our previously reported method. The obtained material was of high purity (>95%) with a correct molecular weight (Supporting Information Fig. S1). The co-assembly strategy was used for triptolide encapsulation, and the influence of C_{16}-N-to-triptolide ratio on the DL and EE of C_{16}-N/T was explored. The DL of C_{16}-N/T increased with increasing triptolide feeding (up to 11%), but the EE dropped significantly meanwhile (Fig. 2A). Quantitative encapsulation was achieved at C_{16}-N-to-triptolide ratio 50:1 (mol/mol) with DL of 1.19 ± 0.07% (in weight, $n = 3$). This C_{16}-N/T was chosen for further experiments, as we have previously observed that high DL could alter the morphology of self-assembled nanofiber and possibly disturb gelation[62]. The C_{16}-N/T was then characterized by TEM and CD. TEM images showed that C_{16}-N and triptolide co-assembled in PBS into nanofibers of 11.0 ± 1.5 nm ($n = 80$) in diameter (Fig. 2B and Supporting Information Fig. S2A), without significant differences in neither the morphology nor diameter when compared with the nanostructures formed by C_{16}-N alone (Fig. S2B). The CD spectrum of C_{16}-N/T nanofiber solution was similar to that of C_{16}-N, showing a negative signal in 216 nm and a positive signal between 285 and 300 nm (derived from tyrosine residues[63]) (Fig. 2C). This result suggested that the peptide segments in C_{16}-N/T nanofibers adopted β-sheet conformation as those in C_{16}-N, and triptolide encapsulation did not affect the molecular packing of C_{16}-N molecules significantly.

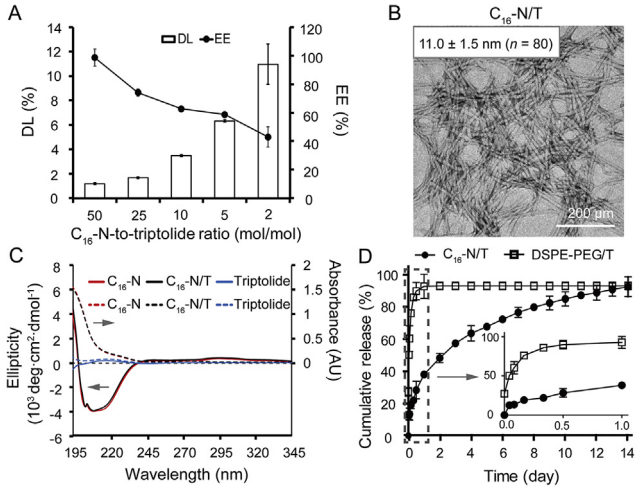

Figure 2 Characterization of C_{16}-N/T. (A) DL and EE of C_{16}-N/T prepared at different C_{16}-N-to-triptolide ratios. (B) Representative TEM image of C_{16}-N/T. (C) CD and UV−VIS spectra of C_{16}-N (500 μmol/L in PBS), C_{16}-N/T (500 μmol/L C_{16}-N and 10 μmol/L triptolide in PBS), and triptolide (10 μmol/L in methanol). (D) Cumulative release of triptolide from C_{16}-N/T and DSPE-PEG/T over 14 days. Data were presented as the mean ± SD (n = 3).

Given that C_{16}-N/T adopted filamentous morphology, they also formed a hydrogel at high concentration only at the presence of salts with a viscosity at ~0.2 Pa·s (Supporting Information Fig. S3). A significant drop in the viscosity was observed after a 5 min stirring (Fig. S3), confirming the shear-thinning properties of the hydrogel we observed previously[54]. The release profile of triptolide from C_{16}-N/T was determined using a Transwell-based methodology. The result showed that the encapsulated triptolide released completely after a 14-day incubation period without obvious burst release, but the rate of drug release declined as prolonged incubation (Fig. 2D). In sharp contrast, DSPE-PEG encapsulated triptolide released in 1 day (Fig. 2D). The effect of DL on drug release was also explored, and similar release profiles were observed from different C_{16}-N/T (DL = 1.22% and 2.15%) (Supporting Information Fig. S4). To verify the stability of released triptolide after prolonged incubation, the molecular mass of released drug at day 6 and day 14 was further confirmed with LC−MS. The peak associated with the released drug showed similar retention time as triptolide with correct molecular mass (Supporting Information Fig. S5), indicating that the triptolide was intact through a 14-day period. In addition to hydrophobic molecules, the supramolecular nature of the C_{16}-N/T allowed feasible entrapment of biomacromolecules within the hydrophilic network formed by C_{16}-N nanofibers through simple mixing procedure. Sustained release of model antibody, Alexa Fluor® 594-labeled lgG, from C_{16}-N-based hydrogel was achieved over a period of 14 days with a burst release phase in the first 8 h, while the complete release was achieved in 1 day for free antibody (Supporting Information Fig. S6). In both cases, most hydrogels retained in the donor chamber at the end of experiments, suggesting that the encapsulated triptolide and entrapped antibody were released mainly through a diffusion-dependent mechanism rather than an erosion-dependent one. The concentration of the encapsulated drug in the nanofibers and its aqueous solubility determined the rate of drug diffusion out of the nanofibers, which explained the decelerated triptolide release as prolonged incubation and faster release of losartan than triptolide from the same nanofibers[54]. Regardless of the exact mechanism of drug release, the results here clearly demonstrated that C_{16}-N-based hydrogel could be an injectable depot for both hydrophobic drugs and biomacromolecules.

3.2. *In vitro study of hydrogel*

We presumed that sustained drug release could allow prolonged drug exposure at tolerable concentration. To test this hypothesis, we monitored the drug uptake and viability of human HCC cell Bel-7402/Luc and human normal liver cell L-02 after their incubation with the release mediums collected at different time points during *in vitro* release experiments using DiI-labeled C_{16}-N (C_{16}-N/DiI) or C_{16}-N/T. Significant and consistent red fluorescence was observed in Bel-7402/Luc cells that were incubated with the release mediums collected at 2 h, day 1, 3 and 11 from C_{16}-N/DiI, while noticeable red fluorescence was only recorded in the cells exposed to the release mediums collected at 2 h and day 1 from DiI-labeled DSPE-PEG (DSPE-PEG/DiI) (Fig. 3A). A similar trend was observed in L-02 cells after incubation with different release mediums, but the fluorescence signals were lower (Fig. 3A). These results were further confirmed quantitatively by flow cytometry analysis (Fig. 3B). The viabilities of cells treated

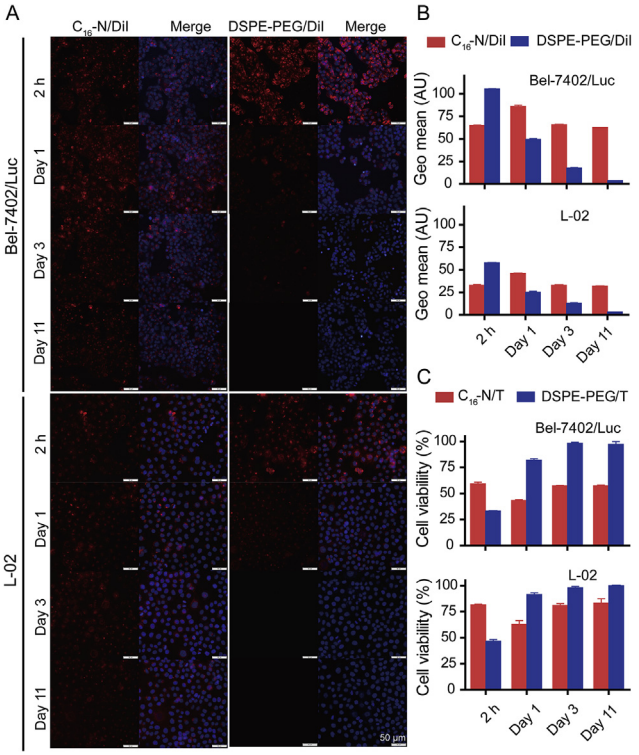

Figure 3 Cell uptake and cytotoxicity of C_{16}-N/T in Bel-7402/Luc and L-02 cells. Fluorescence images (A) and flow cytometry analysis (B) of Bel-7402/Luc and L-02 cells after 12 h incubation with release mediums collected from C_{16}-N/DiI or DSPE-PEG/DiI (Red) at 2 h, day 1, day 3, and day 11. The cell nucleus were stained with Hoechst 33342 (Blue). The scale bars represent a distance of 50 μm. Data were presented as the mean ± SD (n = 3). (C) Viability of Bel-7402/Luc and L-02 cells after 72 h incubation with release mediums collected from C_{16}-N/T or DSPE-PEG/T at 2 h, day 1, day 3, and day 11. Data were presented as the mean ± SD (n = 3).

with diluted release mediums for 72 h were then determined using an MTT-based method. The growth of Bel-7402/Luc cells was inhibited by ~50% after treated with diluted release mediums (2 h, day 1, 3 or 11) from C_{16}-N/T, while the viabilities of L-02 cells were much less affected (Fig. 3C). On the contrary, the release medium collected at 2 h from DSPE-PEG/DiI was toxic to both Bel-7402/Luc and L-02 cells, and those collected at day 1, 3 or 11 were of no activity on both cells (Fig. 3C). In both cases, the activity of released triptolide (20−60 nmol/L) was comparable to that of free triptolide at the same concentration (Supporting Information Fig. S7), confirming that the encapsulated triptolide was stable for at least 14 days. These results proved that C_{16}-N/T could prolong the drug exposure of cancer cells, and indicated that the selective inhibition of cancer cells could be achieved after dosage optimization.

3.3. *Peritoneal retention and distribution of C_{16}-N/T hydrogel*

The behavior of the hydrogel after intraperitoneal injection may be different from that under *in vitro* conditions, due to the movement of animals and internal organs. We, therefore, monitored the intraperitoneal retention and distribution of C_{16}-N/DiR *in vivo* using IVIS spectrum imaging system, and DSPE-PEG/DiR was used as control. The shear-thinning property of the hydrogel was first examined, and fast regelation after vortex and needle injection was observed (Fig. 4A and Supporting Information Fig. S8). After intraperitoneal injection, prolonged retention of C_{16}-N/DiR in the abdomen of the mice was observed, but no significant signal was observed in mice receiving DSPE-PEG/DiR 3 days after the injection (Fig. 4B). Relative fluorescence intensity (RFI) change was further semi-quantified, and the results showed that ~40% of injected DiR remained in the C_{16}-N/DiR treated mice in sharp contrast with <10% in DSPE-PEG/DiR treated ones at the end of experiment (Fig. 4C). The low fluorescence intensity in C_{16}-N/DiR treated mice at day 0 and day 1 was resulted from fluorescence quenching (Fig. S8).

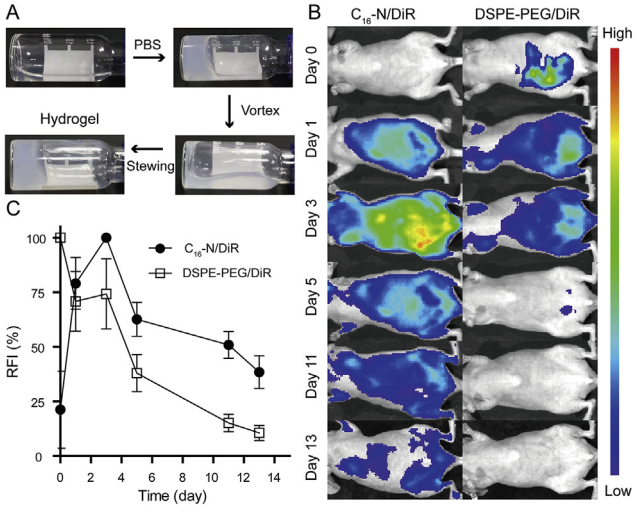

Figure 4 Retention of C_{16}-N hydrogel *in vivo*. (A) Shear-thinning property of C_{16}-N/T. Representative fluorescence images (B) and semi-quantitative analysis of RFI changes (C) of mice receiving either C_{16}-N/DiR or DSPE-PEG/DiR (2 mg/kg DiR) captured at day 0, 1, 3, 5, 11 and 13 after intraperitoneal injection. The total fluorescence intensity was normalized to the highest fluorescence intensity while plotted against time. Data were presented as the mean ± SD (n = 3).

The results confirmed that the injectable hydrogel could also prolong drug exposure *in vivo*. Longer drug retention was observed *in vivo* than *in vitro*, probably due to the limited fluid volume in the intraperitoneal cavity and high affinity of release drugs for the tissues.

We then explored whether prolonged drug exposure after hydrogel injection (i.p.) could lead to higher tissue selectivity of the drug. Therefore, the accumulation of DiR in the major organs and blood of C_{16}-N/DiR-treated mice was monitored and semi-quantified using IVIS spectrum imaging system, and mice receiving DSPE-PEG/DiR *via* intravenous or intraperitoneal injection were used as controls. We found that DiR mainly accumulated in the liver and maintained a stable concentration in mice treated with C_{16}-N/DiR (Supporting Information Fig. S9). The distribution of DSPE-PEG/DiR, on the contrary, showed no obvious tissue specificity and a relative fast clearance when administrated through either intravenous or intraperitoneal injection (Fig. S9). However, the maximal drug exposure in the liver increased and the time-to-peak elongated when DSPE-PEG/DiR was delivered *via* intraperitoneal injection compared with intravenous injection (Fig. S9). The average fluorescence intensities in different organs were semi-quantified and analyzed using organs with known DiR concentration as standards (Supporting Information Fig. S10). The fluorescence intensity change in the liver against time was plotted (Fig. 5A), and the time to reach highest fluorescence intensity (T_{max}) and the areas under the curve (AUC_{0-13}) were calculated (Supporting Information Table S1). DSPE-PEG/DiR (i.v.) and DSPE-PEG/DiR (i.p.) showed comparable AUC_{0-13}, while the AUC_{0-13} of C_{16}-N/DiR was slightly lower as a considerable amount of DiR maintained in the liver at day 13 (Fig. 5A). Tissue-to-liver fluorescence intensity ratios were calculated (0−6 days), and mice treated with C_{16}-N/DiR showed ~2-fold lower heart-to-liver, lungs-to-liver, kidneys-to-liver and blood-to-liver ratios, and slightly higher spleen-to-liver ratio, when compared with mice treated with DSPE-PEG/DiR (Fig. 5B−F). The accumulation of DiR in the spleens of C_{16}-N/DiR-treated mice might be associated with lymphatic clearance of nanofibers and subsequent phagocytosis by macrophages or dendritic cells which could accumulate in the lymph nodes and spleens[25,64]. These results indicated that C_{16}-N hydrogel (i.p.) could deliver encapsulated cargos preferentially to the liver and maintain a steady concentration there for maximized efficacy and minimized side effects.

3.4. *Anti-tumor efficacy of C_{16}-N/T hydrogel*

The anti-tumor activity of C_{16}-N/T was evaluated on orthotopic HCC mice model which was more clinically relevant[65,66]. The mice model established through liver transplantation of Bel-7402/Luc tumor block could be easily monitored using bioluminescence imaging using the IVIS spectrum imaging system with acceptable variance among animals (Supporting Information Fig. S11). The anti-tumor efficacy of C_{16}-N/T (1 mg/kg in triptolide) in the model mice was first monitored using IVIS spectrum imaging system over 2 weeks, and PBS (i.v.), DSPE-PEG/T (i.p. or i.v.), and C_{16}-N (i.p.) at the same dosage were used as control (Fig. 6A and Supporting Information Fig. S12). It was found that the bioluminescence signals increased in mice receiving PBS (i.v.), C_{16}-N (i.p.), DSPE-PEG/T (i.p.) and DSPE-PEG/T (i.v.), but the signals decreased in mice treated with C_{16}-N/T (i.p.) (Fig. 6B). In comparison with PBS, the TIR of C_{16}-N (i.p.) and DSPE-PEG/T (i.v.) were 99.7 ± 0.1% and

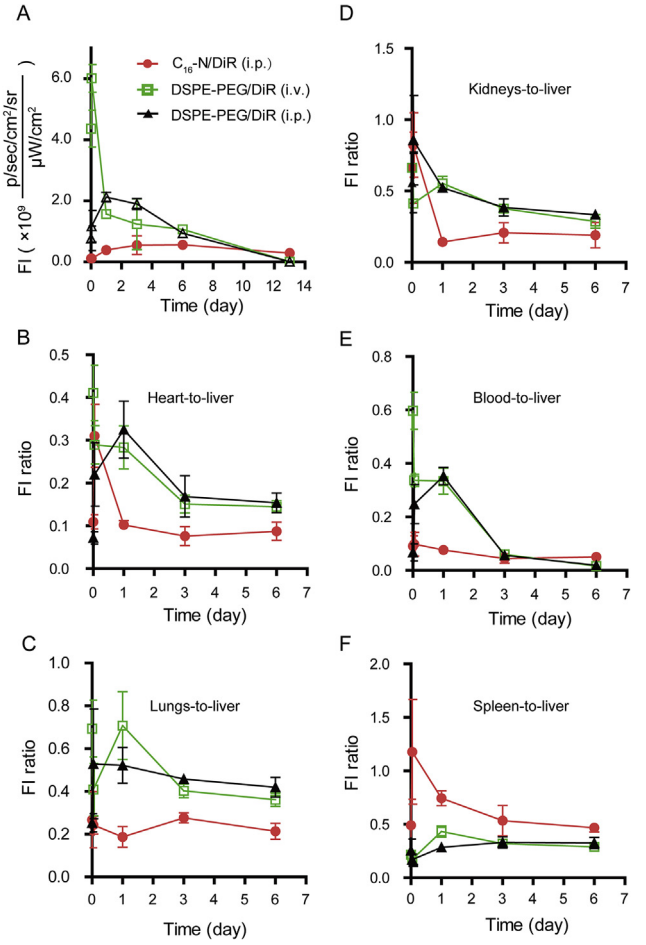

Figure 5 Biodistribution of C_{16}-N hydrogel *in vivo*. (A) Average fluorescence intensity (FI) changes in the livers of mice receiving C_{16}-N/DiR (i.p.), DSPE-PEG/DiR (i.v.), or DSPE-PEG/DiR (i.p.). The organs were collected at 5 min, 1 h, 1 day, 3 days, 6 days, and 13 days after the injection ($n = 3$). The ratios of average FI at 5 min, 1 h, 1 day, 3 days, 6 days in the heart (B), lungs (C), kidneys (D), blood (E), and spleen (F) against that in the livers. Data were presented as mean ± SD ($n = 3$).

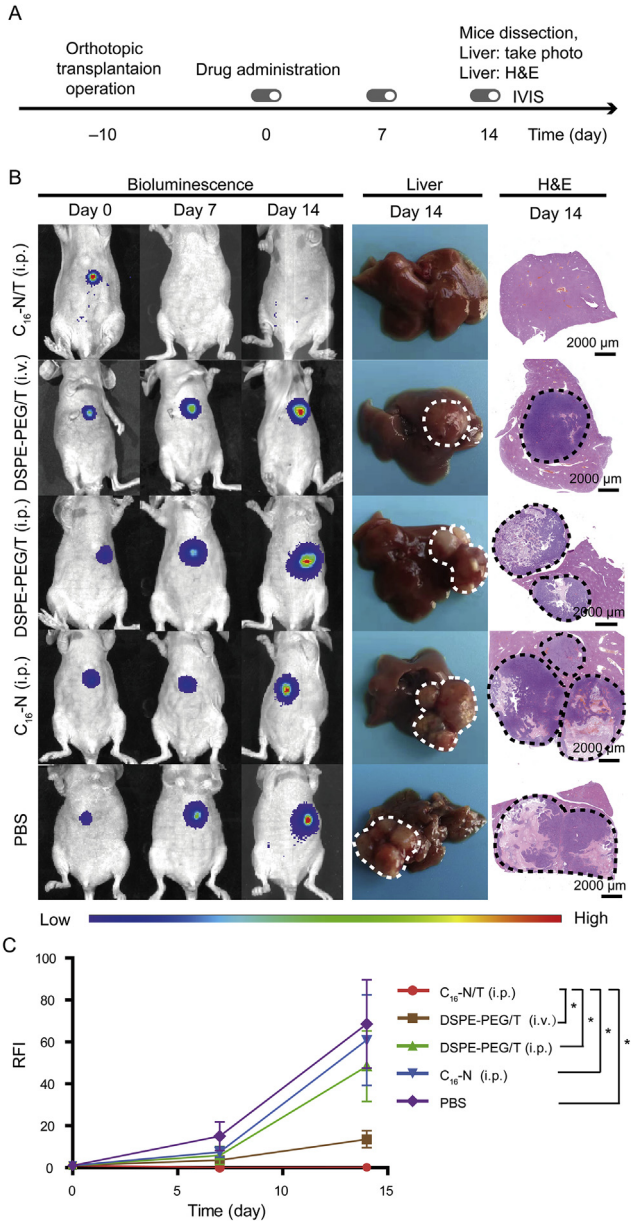

Figure 6 Tumor growth inhibition activity of C_{16}-N/T. (A) Schematic illustration of the experiment design. (B) Representative bioluminescence images of mice captured at day 0, day 7 and day 14 after receiving C_{16}-N/T (i.p.), DSPE-PEG/T (i.v.), DSPE-PEG/T (i.p.), C_{16}-N (i.p.) or PBS. The livers were harvested at the end of experiment, and were imaged, sectioned, and stained using H&E. The tumors were outlined with white dotted line. (C) Semi-quantitative analysis of RFI changes of the same mice. Data were presented as the mean ± SD ($n = 3$). $^{*}P < 0.05$.

80.2 ± 5.9%, respectively. These results were confirmed by further anatomic examination and histological analysis at the end of the experiment (Fig. 6B). Among these triptolide-containing treatments, C_{16}-N/T (i.p.) was the most effective compared with other treatments ($P < 0.05$), followed by DSPE-PEG/T (i.v.) and DSPE-PEG/T (i.p.) (Fig. 6C). Given that DSPE-PEG/T (i.p. or i.v.) have higher AUC_{0-13} than C_{16}-N/T (i.p.) in the liver (Table S1), these results suggested that the span of time was more important than the extent of amount of drug exposure for HCC treatment when effective concentration was reached. Indeed, no significant difference was observed between the mice treated with C_{16}-N/T or DSPE-PEG/T at day 7 (Fig. 6C), before which time an effective drug exposure in the liver maintained (Fig. 5A). In the second week, an effective concentration of drug maintained only in the liver of mice receiving C_{16}-N/T hydrogel (Fig. 5A), which led to superior activity in inhibiting the growth of orthotopic tumors.

To further investigate the long-term efficacy of C_{16}-N/T hydrogel, a survival experiment was performed with the same control groups ($n = 8$ for each group). C_{16}-N/T hydrogel was the most effective among all the treatments, and the median survival times were 43, 24, 22, 22, and 19 days for C_{16}-N/T (i.p.), DSPE-PEG/T (i.v.), DSPE-PEG/T (i.p.), C_{16}-N (i.p.), and PBS (i.v.) treated mice, respectively (Fig. 7A). In the first 2 weeks after drug administration, body weight loss >10% was not observed in mice except those receiving DSPE-PEG/T (i.v., 12.54%) (Fig. 7B). The body weight loss observed after that was usually associated with tumor progression. The results here were in consistent with the bioluminescence imaging result (Fig. 6), showing that C_{16}-N/T (i.p.) was the most effective treatment

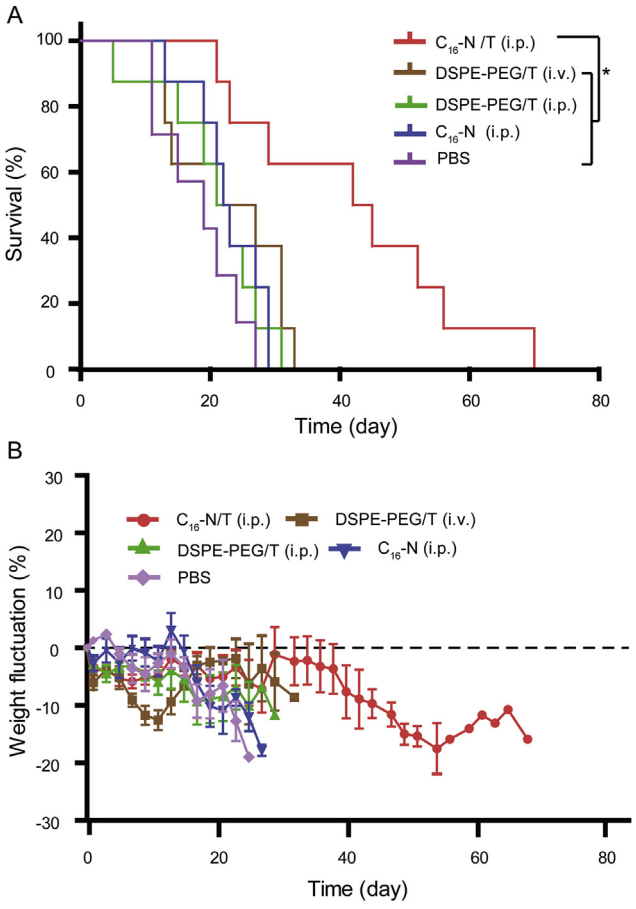

Figure 7 The survival and body weight changes of mice after treatments. Survival curve (A) and body weight changes (B) of mice receiving C_{16}-N/T (i.p.), DSPE-PEG/T (i.v.), DSPE-PEG/T (i.p.), C_{16}-N (i.p.) or PBS ($n = 8$). Data were presented as mean ± SD $^{*}P < 0.05$.

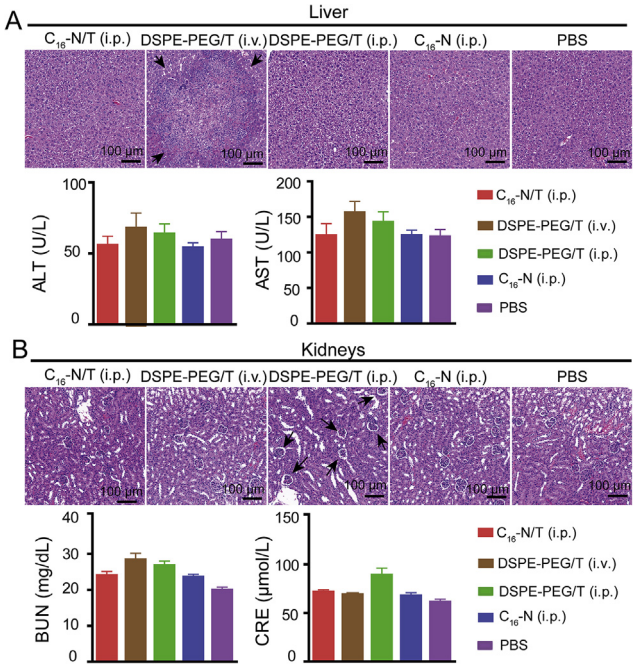

Figure 8 Safety assessment on C_{16}-N/T hydrogel. (A) Representative images of livers and serum activities of ALT and AST collected from mice 4 days after receiving C_{16}-N/T (i.p.), DSPE-PEG/T (i.v.), DSPE-PEG/T (i.p.), C_{16}-N (i.p.) or PBS ($n = 3$). The damages in the liver were indicated by black arrows. (B) Representative images of kidneys and serum concentrations of BUN and CRE. The damages in renal corpuscles were indicated by black arrows. Data were presented as the mean ± SD ($n = 3$).

in treating orthotopic HCC-bearing mice. The observed body weight loss of mice receiving DSPE-PEG/T (i.v.) indicated that the treatment had significant side effects on major organs due to high drug exposure (Fig. 5 and Fig. S9), which might explain why tumor growth inhibition did not translate into survival benefit in mice receiving DSPE-PEG/T (i.v.) (Figs. 6 and 7).

3.5. *Safety of the C_{16}-N/T hydrogel*

To further investigate the *in vivo* safety of C_{16}-N/T, the histological change in the major organs and blood biochemical parameters were examined on healthy Balb/c nude mice at day 4 after receiving different treatments. No obvious histological changes were observed in the heart, spleen and lungs of mice receiving any of the treatments (Supporting Information Fig. S13). However, liver tissue necrosis and inflammation were observed in one of the three mice receiving DSPE-PEG/T (i.v.) (Fig. 8A). Further blood biochemical parameter analysis showed that mice receiving DSPE-PEG/T (i.v.) or DSPE-EPG/T (i.p.) had elevated activities of ALT and AST when compared with those receiving PBS, C_{16}-N, or C_{16}-N/T (Fig. 8A). The kidneys of the mice were also analyzed, and histological change in the renal corpuscles was observed in all of the three mice receiving DSPE-EPG/T (i.p.) but not in the rest mice, with widened corpuscle space and glomerulus necrosis (Fig. 8B). In agreement with this result, elevated CRE was recorded only in mice receiving DSPE-EPG/T (i.p.) (Fig. 8B). Elevated BUN was observed in all other groups compared with PBS-treated mice, and thus might not be associated with triptolide treatment (Fig. 8B). The results here demonstrated that C_{16}-N/T hydrogel (i.p.) was better tolerated than DSPE-PEG/T, which was resulted from its prolonged drug release and liver specific accumulation (Figs. 4 and 5).

4. Conclusions

In this study, we explored the potential of C_{16}-N hydrogel as an intraperitoneal depot for triptolide for the treatment of orthotopic HCC. We showed that triptolide could be quantitatively loaded into C_{16}-N nanofibers, and drug encapsulation did not affect self-assembly and gelation. Triptolide released from C_{16}-N/T hydrogel sustainedly, and showed higher cytotoxicity against HCC cells than normal hepatocytes. After intraperitoneal injection, the hydrogel retained in the peritoneal cavity for more than 2 weeks, with preferential accumulation in the liver. The C_{16}-N/T hydrogel significantly inhibited the growth of orthotopic HCC growth, and doubled the median survival time of tumor-bearing mice without noticeable side effects to major organs. Our findings clearly demonstrated that C_{16}-N/T hydrogel has a strong potential in HCC chemotherapy and combined therapy.

Acknowledgments

We thank the National Natural Science Foundation of China (Nos. 81690265, 31870995, 81671808 and 81630052),Youth Innovation Promotion Association of the Chinese Academy of Sciences (2017335, China), and SA-SIBS Scholarship Program for financial support (China). We are grateful to National Centre for Protein Science Shanghai (Electron Microscopy system) for instrument support and technical assistance during data collection.

Appendix A. Supporting information

Supporting data to this article can be found online at https://doi.org/10.1016/j.apsb.2019.06.001.

References

1. Wang HD, Naghavi M, Allen C, Barber RM, Bhutta ZA, Carter A, et al. Global, regional, and national life expectancy, all-cause mortality, and cause-specific mortality for 249 causes of death, 1980–2015: a systematic analysis for the global burden of disease study 2015. *Lancet* 2016;**388**:1459−544.
2. Torre LA, Bray F, Siegel RL, Ferlay J, Lortet-Tieulent J, Jemal A. Global cancer statistics. *CA A Cancer J Clin* 2012;**65**:87−108. 2015.
3. Llovet JM, Villanueva A, Lachenmayer A, Finn RS. Advances in targeted therapies for hepatocellular carcinoma in the genomic era. *Nat Rev Clin Oncol* 2015;**12**:408−24.
4. Fu J, Wang H. Precision diagnosis and treatment of liver cancer in China. *Cancer Lett* 2018;**412**:283−8.
5. Forner A, Gilabert M, Bruix J, Raoul JL. Treatment of intermediate-stage hepatocellular carcinoma. *Nat Rev Clin Oncol* 2014;**11**:525−35.
6. Llovet JM, Ricci S, Mazzaferro V, Hilgard P, Gane E, Blanc JF, et al. Sorafenib in advanced hepatocellular carcinoma. *N Engl J Med* 2008;**359**:378−90.
7. Zhu AX, Finn RS, Edeline J, Cattan S, Ogasawara S, Palmer D, et al. Pembrolizumab in patients with advanced hepatocellular carcinoma previously treated with sorafenib (KEYNOTE-224): a non-randomised, open-label phase 2 trial. *Lancet Oncol* 2018;**19**:940−52.
8. Zaanan A, Williet N, Hebbar M, Dabakuyo TS, Fartoux L, Mansourbakht T, et al. Gemcitabine plus oxaliplatin in advanced hepatocellular carcinoma: a large multicenter AGEO study. *J Hepatol* 2013;**58**:81−8.
9. Phillips PA, Dudeja V, McCarroll JA, Borja-Cacho D, Dawra RK, Grizzle WE, et al. Triptolide induces pancreatic cancer cell death *via* inhibition of heat shock protein 70. *Cancer Res* 2007;**67**:9407−16.
10. Mujumdar N, Mackenzie TN, Dudeja V, Chugh R, Antonoff MB, Borja-Cacho D, et al. Triptolide induces cell death in pancreatic cancer cells by apoptotic and autophagic pathways. *Gastroenterology* 2010;**139**:598−608.
11. Ling D, Xia H, Park W, Hackett MJ, Song C, Na K, et al. pH-Sensitive nanoformulated triptolide as a targeted therapeutic strategy for hepatocellular carcinoma. *ACS Nano* 2014;**8**:8027−39.
12. Peer D, Karp JM, Hong S, FaroKHzad OC, Margalit R, Langer R. Nanocarriers as an emerging platform for cancer therapy. *Nat Nanotechnol* 2007;**2**:751−60.
13. Liang Y, Tian B, Zhang J, Li K, Wang L, Han J, et al. Tumor-targeted polymeric nanostructured lipid carriers with precise ratiometric control over dual-drug loading for combination therapy in non-small-cell lung cancer. *Int J Nanomed* 2017;**12**:1699−715.
14. Tsoi KM, MacParland SA, Ma XZ, Spetzler VN, Echeverri J, Ouyang B, et al. Mechanism of hard-nanomaterial clearance by the liver. *Nat Mater* 2016;**15**:1212−21.
15. Ashley CE, Carnes EC, Phillips GK, Padilla D, Durfee PN, Brown PA, et al. The targeted delivery of multicomponent cargos to cancer cells by nanoporous particle-supported lipid bilayers. *Nat Mater* 2011;**10**:389−97.
16. Lu J, Wang J, Ling D. Surface engineering of nanoparticles for targeted delivery to hepatocellular carcinoma. *Small* 2018;**14**:1702037.
17. Xia H, Li F, Hu X, Park W, Wang S, Jang Y, et al. pH-Sensitive Pt nanocluster assembly overcomes cisplatin resistance and heterogeneous stemness of hepatocellular carcinoma. *ACS Cent Sci* 2016;**2**:802−11.
18. Lu J, Sun J, Li F, Wang J, Liu J, Kim D, et al. Highly sensitive diagnosis of small hepatocellular carcinoma using pH-responsive iron oxide nanocluster assemblies. *J Am Chem Soc* 2018;**140**:10071−4.
19. Chi Y, Yin X, Sun K, Feng S, Liu J, Chen D, et al. Redox-sensitive and hyaluronic acid functionalized liposomes for cytoplasmic drug delivery to osteosarcoma in animal models. *J Control Release* 2017;**261**:113−25.
20. Docter D, Westmeier D, Markiewicz M, Stolte S, Knauer SK, Stauber RH. The nanoparticle biomolecule corona: lessons learned-challenge accepted?. *Chem Soc Rev* 2015;**44**:6094−121.
21. Markman M. Intraperitoneal antineoplastic drug delivery: rationale and results. *Lancet Oncol* 2003;**4**:277−83.
22. Lin G, Lunderquist A, Hägerstrand I, Boijsen E. Postmortem examination of the blood supply and vascular pattern of small liver metastases in man. *Surgery* 1984;**96**:517−26.
23. Werner ME, Karve S, Sukumar R, Cummings ND, Copp JA, Chen RC, et al. Folate-targeted nanoparticle delivery of chemo- and radiotherapeutics for the treatment of ovarian cancer peritoneal metastasis. *Biomaterials* 2011;**32**:8548−54.
24. Deng Y, Yang F, Cocco E, Song E, Zhang J, Cui J, et al. Improved i.p. drug delivery with bioadhesive nanoparticles. *Proc Natl Acad Sci U S A* 2016;**113**:11453−8.
25. Parker RJ, Hartman KD, Sieber SM. Lymphatic absorption and tissue disposition of liposome-entrapped [^{14}C]adriamycin following intraperitoneal administration to rats. *Cancer Res* 1981;**41**:1311−7.
26. Lukas G, Brindle SD, Greengard P. The route of absorption of intraperitoneally administered compounds. *J Pharmacol Exp Ther* 1971;**178**:562−6.
27. Li J, Mooney DJ. Designing hydrogels for controlled drug delivery. *Nat Rev Mater* 2016;**1**:16071.
28. Gao W, Vecchio D, Li J, Zhu J, Zhang Q, Fu V, et al. Hydrogel containing nanoparticle-stabilized liposomes for topical antimicrobial delivery. *ACS Nano* 2014;**8**:2900−7.
29. Bajaj G, Kim MR, Mohammed SI, Yeo Y. Hyaluronic acid-based hydrogel for regional delivery of paclitaxel to intraperitoneal tumors. *J Control Release* 2012;**158**:386−92.
30. Sato K, Hendricks MP, Palmer LC, Stupp SI. Peptide supramolecular materials for therapeutics. *Chem Soc Rev* 2018;**47**:7539−51.
31. Goor OJ, Hendrikse SI, Dankers PY, Meijer EW. From supramolecular polymers to multi-component biomaterials. *Chem Soc Rev* 2017;**46**:6621−37.
32. Jonker AM, Lowik DW, van Hest JC. Peptide- and protein-based hydrogels. *Chem Mater* 2012;**24**:759−73.
33. Smith DJ, Brat GA, Medina SH, Tong D, Huang Y, Grahammer J, et al. A multiphase transitioning peptide hydrogel for suturing ultrasmall vessels. *Nat Nanotechnol* 2016;**11**:95−102.
34. Moore AN, Hartgerink JD. Self-assembling multidomain peptide nanofibers for delivery of bioactive molecules and tissue regeneration. *Acc Chem Res* 2017;**50**:714−22.
35. Koutsopoulos S, Unsworth LD, Nagai Y, Zhang S. Controlled release of functional proteins through designer self-assembling peptide nanofiber hydrogel scaffold. *Proc Natl Acad Sci U S A* 2009;**106**:4623−8.
36. Asai D, Xu D, Liu W, Garcia Quiroz F, Callahan DJ, Zalutsky MR, et al. Protein polymer hydrogels by *in situ*, rapid and reversible self-gelation. *Biomaterials* 2012;**33**:5451−8.
37. Nowak AP, Breedveld V, Pakstis L, Ozbas B, Pine DJ, Pochan D, et al. Rapidly recovering hydrogel scaffolds from self-assembling diblock copolypeptide amphiphiles. *Nature* 2002;**417**:424−8.
38. Fichman G, Gazit E. Self-assembly of short peptides to form hydrogels: design of building blocks, physical properties and technological applications. *Acta Biomater* 2014;**10**:1671−82.

39. Frederix PW, Scott GG, Abul-Haija YM, Kalafatovic D, Pappas CG, Javid N, et al. Exploring the sequence space for (tri-)peptide self-assembly to design and discover new hydrogels. *Nat Chem* 2015;**7**:30−7.
40. O'Leary LE, Fallas JA, Bakota EL, Kang MK, Hartgerink JD. Multi-hierarchical self-assembly of a collagen mimetic peptide from triple helix to nanofibre and hydrogel. *Nat Chem* 2011;**3**:821−8.
41. Tanrikulu IC, Forticaux A, Jin S, Raines RT. Peptide tessellation yields micrometre-scale collagen triple helices. *Nat Chem* 2016;**8**:1008−14.
42. Yan C, Pochan DJ. Rheological properties of peptide-based hydrogels for biomedical and other applications. *Chem Soc Rev* 2010;**39**:3528−40.
43. Clarke DE, Parmenter CD, Scherman OA. Tunable pentapeptide self-assembled β-sheet hydrogels. *Angew Chem Int Ed Engl* 2018;**57**:7709−13.
44. De Leon Rodriguez LM, Hemar Y, Cornish J, Brimble MA. Structure-mechanical property correlations of hydrogel forming β-sheet peptides. *Chem Soc Rev* 2016;**45**:4797−824.
45. Du X, Zhou J, Shi J, Xu B. Supramolecular hydrogelators and hydrogels: from soft matter to molecular biomaterials. *Chem Rev* 2015;**115**:13165−307.
46. Fu IW, Markegard CB, Nguyen HD. Solvent effects on kinetic mechanisms of self-assembly by peptide amphiphiles *via* molecular dynamics simulations. *Langmuir* 2015;**31**:315−24.
47. Li YL, Rodrigues J, Tomás H. Injectable and biodegradable hydrogels: gelation, biodegradation and biomedical applications. *Chem Soc Rev* 2012;**41**:2193−221.
48. Pashuck ET, Duchet BJ, Hansel CS, Maynard SA, Chow LW, Stevens MM. Controlled sub-nanometer epitope spacing in a three-dimensional self-assembled peptide hydrogel. *ACS Nano* 2016;**10**:11096−104.
49. Li J, Zhan Z, Du X, Wang J, Hong B, Xu B. Selection of secondary structures of heterotypic supramolecular peptide assemblies by an enzymatic reaction. *Angew Chem Int Ed Engl* 2018;**57**:11716−21.
50. Shi J, Fichman G, Schneider JP. Enzymatic control of the conformational landscape of self-assembling peptides. *Angew Chem Int Ed Engl* 2018;**57**:11188−92.
51. Zhou J, Du X, Gao Y, Shi J, Xu B. Aromatic-aromatic interactions enhance interfiber contacts for enzymatic formation of a spontaneously aligned supramolecular hydrogel. *J Am Chem Soc* 2014;**136**:2970−3.
52. Chen ZP, Xing L, Fan Q, Cheetham AG, Lin R, Holt B, et al. Drug-bearing supramolecular filament hydrogels as anti-inflammatory agents. *Theranostics* 2017;**7**:2003−14.
53. Cheetham AG, Zhang PC, Lin YA, Lock LL, Cui HG. Supramolecular nanostructures formed by anticancer drug assembly. *J Am Chem Soc* 2013;**135**:2907−10.
54. Hu C, Liu X, Ran W, Meng J, Zhai YH, Zhang PC, et al. Regulating cancer associated fibroblasts with losartan-loaded injectable peptide hydrogel to potentiate chemotherapy in inhibiting growth and lung metastasis of triple negative breast cancer. *Biomaterials* 2017;**144**:60−72.
55. Edelbrock AN, Àlvarez Z, Simkin D, Fyrner T, Chin SM, Sato K, et al. Supramolecular nanostructure activates TrkB receptor signaling of neuronal cells by mimicking brain-derived neurotrophic factor. *Nano Lett* 2018;**18**:6237−47.
56. Freeman R, Han M, Álvarez Z, Lewis JA, Wester JR, Stephanopoulos N, et al. Reversible self-assembly of superstructured networks. *Science* 2018;**362**:808−13.
57. Li IC, Hartgerink JD. Covalent capture of aligned self-assembling nanofibers. *J Am Chem Soc* 2017;**139**:8044−50.
58. Lock LL, Lo YG, Mao XP, Chen HW, Staedtke V, Bai RY, et al. One-component supramolecular filament hydrogels as theranostic label-free magnetic resonance imaging agents. *ACS Nano* 2017;**11**:797−805.
59. Jensen G, Morrill C, Huang Y. 3D tissue engineering, an emerging technique for pharmaceutical research. *Acta Pharm Sin B* 2018;**8**:756−66.
60. Wagner AM, Gran MP, Peppas NA. Designing the new generation of intelligent biocompatible carriers for protein and peptide delivery. *Acta Pharm Sin B* 2018;**8**:147−64.
61. Zhai Y, Ran W, Su J, Lang T, Meng J, Wang G, et al. Traceable bioinspired nanoparticle for the treatment of metastatic breast cancer *via* NIR-trigged intracellular delivery of methylene blue and cisplatin. *Adv Mater* 2018;**30**:1802378.
62. Zhang P, Cheetham AG, Lin YA, Cui H. Self-Assembled Tat nanofibers as effective drug carrier and transporter. *ACS Nano* 2013;**7**:5965−77.
63. Zaidi S, Hassan MI, Islam A, Ahmad F. The role of key residues in structure, function, and stability of cytochrome-*c*. *Cell Mol Life Sci* 2014;**71**:229−55.
64. Creusot RJ, Yaghoubi SS, Chang P, Chia J, Contag CH, Gambhir SS, et al. Lymphoid-tissue-specific homing of bone-marrow-derived dendritic cells. *Blood* 2009;**113**:6638−47.
65. Talmadge JE, Singh RK, Fidler IJ, Raz A. Murine models to evaluate novel and conventional therapeutic strategies for cancer. *Am J Pathol* 2007;**170**:793−804.
66. Wang Q, Zhang P, Li Z, Feng X, Lv C, Zhang H, et al. Evaluation of polymer nanoformulations in hepatoma therapy by established rodent models. *Theranostics* 2019;**9**:1426−52.